Kirscher, U., et al., 2020, Paleomagnetic constraints on the duration of the Australia-Laurentia connection in the core of the Nuna supercontinent: Geology, v. 49, https://doi.org/10.1130/G47823.1

Supplementary Materials for

Paleomagnetic constraints on the duration of the Australia–Laurentia connection in the core of the Nuna supercontinent

Uwe Kirscher, Ross N. Mitchell, Yebo Liu, Adam R. Nordsvan, Grant M. Cox, Sergei A. Pisarevsky, Chong Wang, Lei Wu, J. Brendan Murphy, and Zheng-Xiang Li

This PDF file includes:

Supplementary methods

Figures S1 to S5

Tables S1 to S7

SUPPLEMENTARY TEXT

Sampling details of Derim Derim sill outcrops

No contact with the Roper Group strata was visible in any sampled outcrop. Accordingly, the stratigraphic positions of the sampled sills were based on the most recent geological map (Abbott et al., 2001), which suggests that the sampled Derim Derim sills intruded the Jalobi Formation (sites DD1), the Sherwin Formation (DD2), the Kyalla Formation (DD3, 4, 5, 13), the Hodgson Sandstone and Corcoran Formation (DD9) and the Crawford Formation (DD10, 11, 12).

Detailed paleomagnetic and rock magnetic methods

Block samples were oriented with both magnetic and sun compasses. Sun-compass observations were made whenever possible to ensure an accurate measure of the local magnetic declination. From the six to eight oriented block samples from each site, inch-diameter cores were drilled in the laboratory and cut in standard sized cylinders. Magnetizations were measured with a 2G-Enterprises DC SQuID magnetometer with background noise sensitivity of ~5×10^{-12} Am² per axis at Curtin University. The magnetometer is equipped with computer controlled, online alternating-field demagnetization coils and an automated vacuum pick-and-put sample-changing array (Kirschvink et al., 2008). Samples and instruments are housed in a magnetically shielded room with residual fields less than 500 nT throughout the demagnetization procedures.

To obtain information on the magnetic carriers three rock magnetic experiments were conducted: a composite 3-axis isothermal remanent magnetization was thermally demagnetized (Lowrie, 1990), additionally susceptibility vs temperature curves, and magnetic hysteresis loops were obtained. Susceptibility vs temperature curves were obtained using an AGICO MFK1-FA Kappabridge in both argon and air atmospheres; magnetic hysteresis loops were obtained using a variable field translation balance.

All samples were subjected to 15 minutes of low-temperature cleaning in a liquid nitrogen bath to remove potential contamination of “soft” magnetic components carried by multi-

domain magnetite (Schmidt, 1993). Thermal demagnetization proceeded in steps of 10–50 °C up to 600 °C (or until thoroughly demagnetized or unstable, for an average of 20 steps per specimen) in a magnetically shielded ASC furnace (±2 °C error). AF demagnetization proceeded in steps of 5-20 mT up to 110 mT (or until thoroughly demagnetized or unstable, for an average of 20 steps per specimen). Magnetic components were computed for each sample using principal-component analysis (Kirschvink, 1980) as implemented in Paleomag OS X (Jones, 2002). All vectors were calculated using at least four successive steps with a maximum angular deviation (MAD) < 10°. In instances where stable-endpoints could not be reached, remagnetization great circles were fitted. Site-mean directions and mean virtual geomagnetic poles (VGPs) were calculated using Fisher statistics (Fisher, 1953) or the iterative approach combining great circles and magnetic vectors (McFadden & McElhinny, 1988). All calculations were carried out using the PmagPy package (Tauxe et al., 2016). GPlates software (Boyden et al., 2011) was used for paleogeographic reconstruction.

Nearly all samples carry a low-temperature/low-coercivity component typically stable up to 300°C (occasionally 550°C) and 20 mT, respectively (Fig. 1). This low-stability component of the Derim Derim samples yields a mean direction indistinguishable from that of the present-day magnetic field for this region and is therefore explained by a recent overprint (Fig. S4). Great circles were only added to calculate mean ChRM directions of two of the 12 sites (Table S3, Fig. S4). Both sedimentary sites from drill core sampled for a baked contact test exhibit stable demagnetization behavior (Fig. S4)).

Reversal Test

We carried out a set of tests to see if the directions might reveal a positive reversal test. This has proved to be slightly problematic because only one site shows a reversed polarity. The reversal test of Mcfadden and Mcelhinny (1990) yields an indeterminate result with the angle between the normal polarity mean direction and the revered mean direction being 11.7°. Nonetheless, after flipping one polarity, the two directions do overlap within uncertainty (Fig. S4). A Watson test also reveals that the directions of the two polarities could have been drawn from the same population. More data is needed for a robust test, but we conclude that the two polarities can be interpreted as being representative of the presence of a geomagnetic field reversal.

Secular Variation

Combining the site mean direction to an overall mean direction yields a secular variation value of S=21.51. A recent compilation of high-quality data (Veikkolainen and Pesonen, 2014) suggests S values in the Precambrian in the range of 5-15 for a paleolatitude of ~25°. The value for the Derim Derim sills is elevated but not unreasonably so. Also, the Deenen criteria (Deenen et al., 2011) shows a value within the expected range of secular variations. Both these aspects do suggest that secular variation has been sufficiently averaged out, but large uncertainties remain related to the extent of secular variation expected in the Mesoproterozoic.

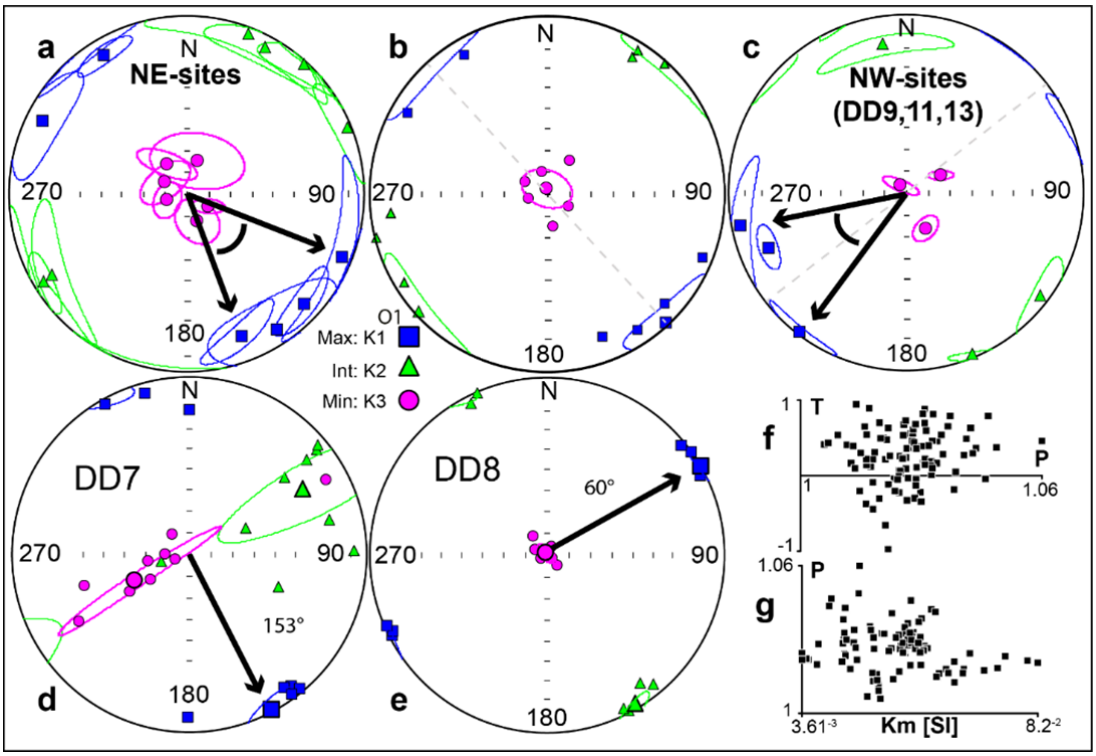

Figure S1. Results of anisotropy of magnetic susceptibility (AMS). (a) Mean anisotropy of magnetic susceptibility tensor of Derim Derim sill sites with a south-easterly lineation direction (DD2, 4, 5, 10, 12) with according confidence ellipses. (b) Mean directions of sites of (a) with the overall mean tensor of these sites. (c) Mean tensor of site with south-westerly lineation direction (DD9, 11, 13). Black arrows indicate variation of lineation direction within these sites. (d+e) AMS results with mean tensor of both drill core sites. (f+g) Plots of degree of anisotropy (P) versus mean susceptibility (Km) and shape parameter (T) versus P for all measured samples.

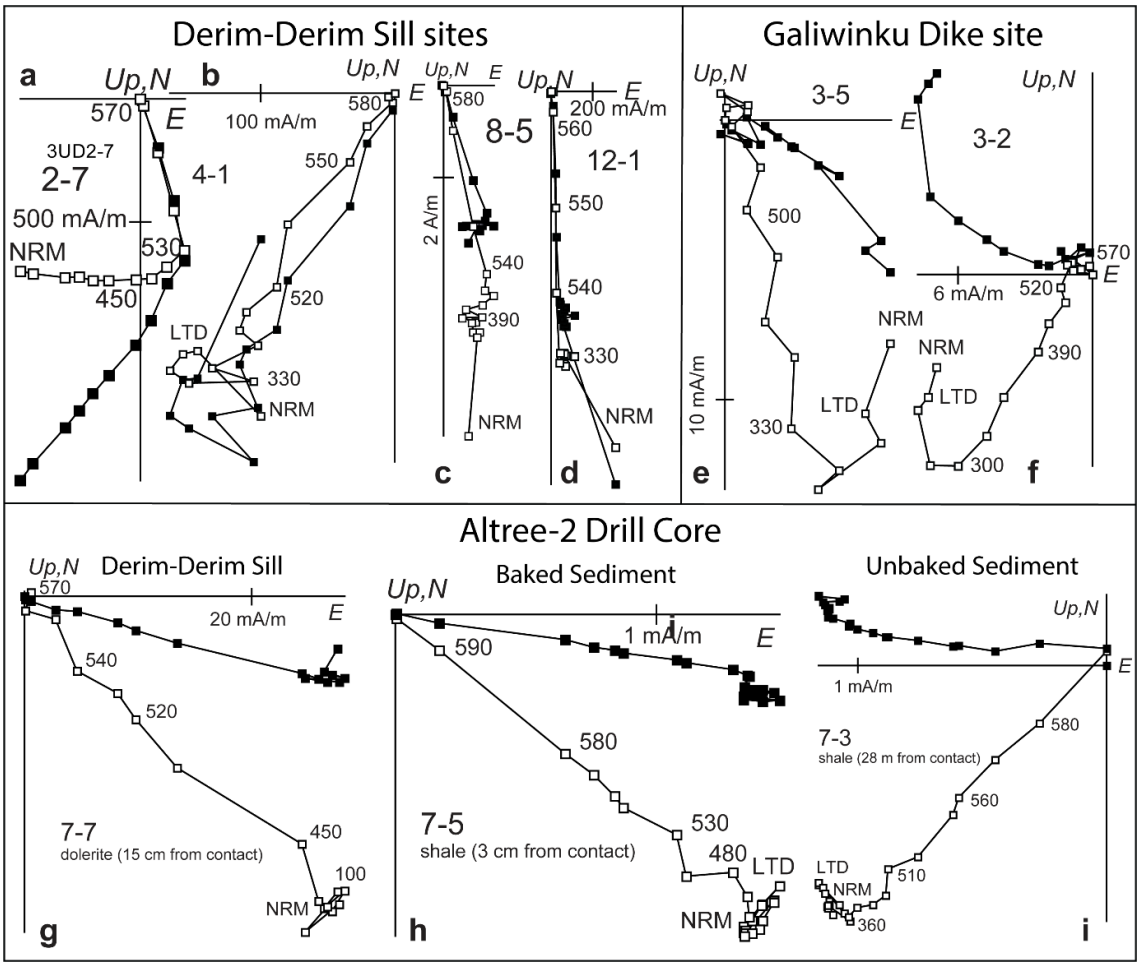

Figure S2. Representative demagnetization plots in orthogonal vector endpoint diagrams (Zijderveld, 1967). Open/filled symbols indicate projections on the horizontal/vertical planes. Demagnetization steps are given in °C, if not otherwise indicated. (a-d+g) represent Derim Derim sill samples, (e+f) Galiwinku dyke samples, (g-i) contact sediments and Derim Derim sill samples from the Altree-2 drill core. LTD refers to an initial low temperature step in liquid nitrogen.

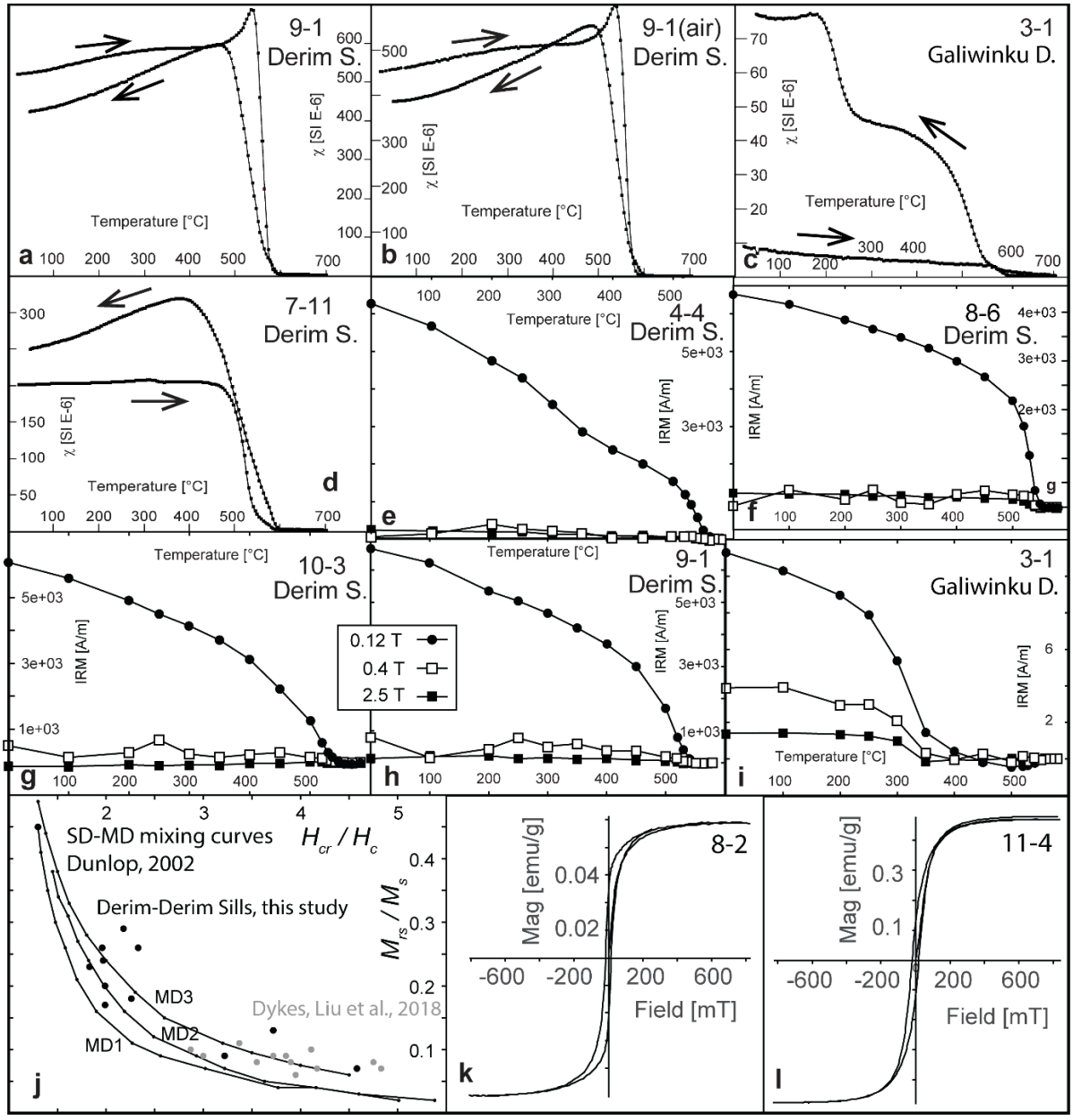

Figure S3. Representative rock magnetic results. (a-d) Susceptibility versus temperature curves; (e-i) Progressive thermal demagnetization of three-axis composite IRMs, (j-l) magnetic hysteresis loops.

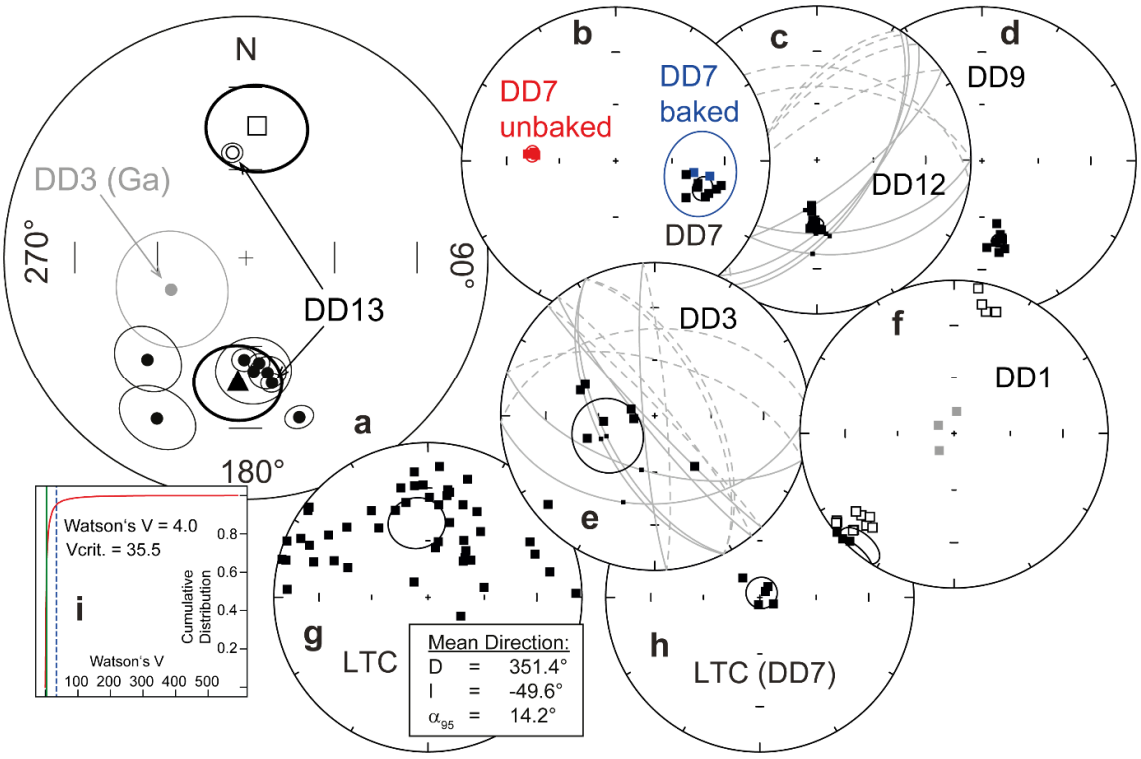

Figure S4. Equal-area stereonets showing (a) the site-mean directions of ChRM of the Derim Derim sill sites and the Galiwinku dyke site (Ga, DD3). Reversed polarity site DD13 is shown in its original (open circle) and flipped (filled circle) orientation. Filled triangle is overall mean of the Derim Derim sill sites including DD13, and the open square represents the mirrored normal polarity mean direction, showing the overlap between the normal polarity sites and reverse polarity site DD13. (b) All directions of drill core site DD7 including the baked contact test; (c-f) Sample and site mean directions with site mean error intervals of sites DD1, 3, 9, 12. (g-h) LTC of Derim Derim sill outcrop sites (g) and drill core site DD7 (h). (h) A steep overprint direction likely representing a drilling-induced remanence. Filled symbols indicate lower hemisphere directions. (i) Watson's test of common mean on Derim Derim sill mean directions with normal and reverse polarities (see supplementary text for more explanation).

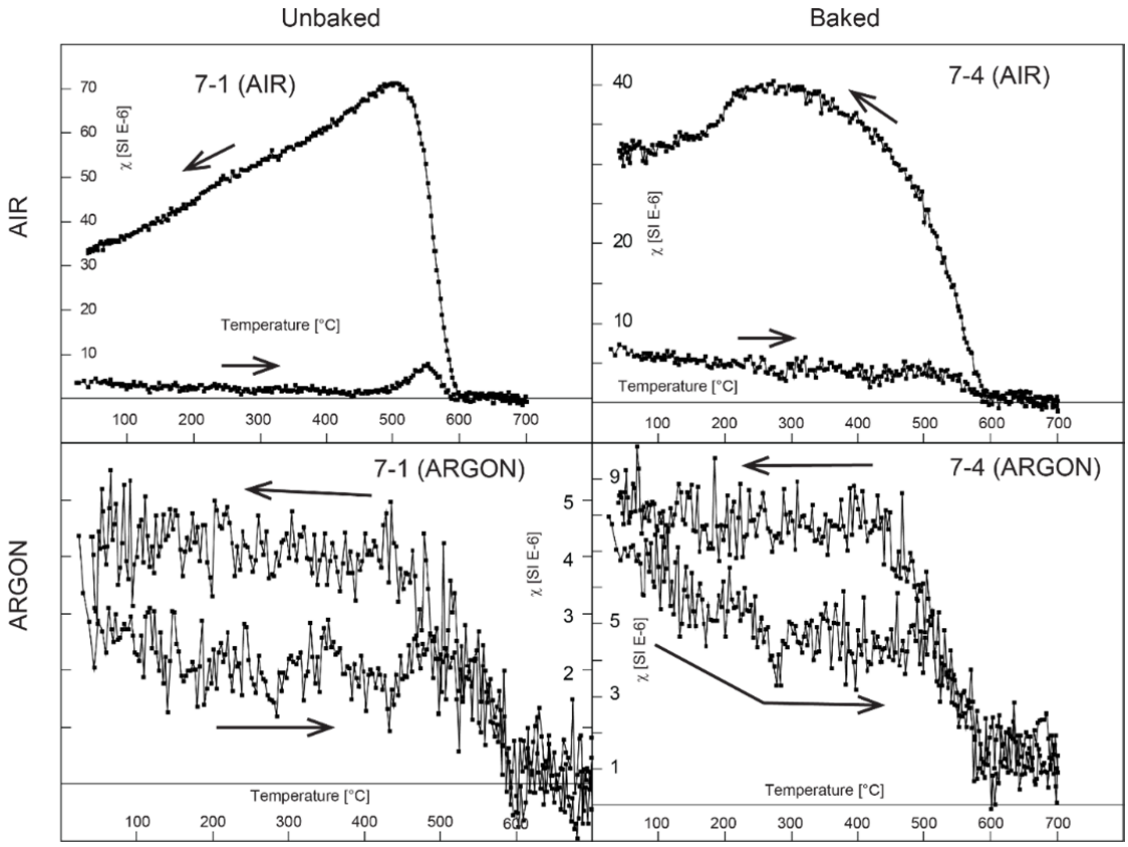

Figure S5. Susceptibility versus temperature curves of baked and unbaked sediment overlying Derim Derim sills from the Altree-2 drill core. Experiments were performed in air and argon atmospheres. Sample 7-1 is from ca. 30 m above the contact to the sills, whereas 7-4 is ca. 10 cm from above the contact (see main text for further explanation). Heating and subsequent cooling cycles are shown indicated by black arrows.

Table S1. GPS coordinates of the sampling sites and drill cores.

Site DD-	Latitude	Longitude	Sampling environment
1	-14.708	134.443	Derim Derim Sill outcrop
2	-14.705	134.296	Derim Derim Sill outcrop
3	-14.736	134.259	Galiwinku Dike outcrop
4	-14.760	134.212	Derim Derim Sill outcrop
5	-14.819	134.131	Derim Derim Sill outcrop
7	-15.924	133.787	Derim Derim Sill drill core (Altree-2)
8	-15.632	132.826	Derim Derim Sill drill core (Tarlee-S3)
9	-14.252	133.663	Derim Derim Sill outcrop
10	-14.121	133.889	Derim Derim Sill outcrop
11	-14.074	134.035	Derim Derim Sill outcrop
12	-14.186	133.804	Derim Derim Sill outcrop
13	-14.928	134.033	Derim Derim Sill outcrop

Table S2. AMS results of the Derim Derim sills and Galiwinku dyke (DD3).

			Max			Int			Min			Average			
Site	N	Kmean [SI]	Dec [°]	Inc [°]	Conf.angle	Dec [°]	Inc [°]	Conf.angle	Dec [°]	Inc [°]	Conf.angle	Lmean	Fmean	Pjmean	Tmean
DD1	10	5.37E-02	165.3	10.6	8.4/2.2	255.3	0.4	9.5/7.3	347.4	79.4	8.5/2.2	1.007	1.009	1.016	0.075
DD2	6	2.54E-02	132.9	11.1	15.2/7	42.3	2.8	18.1/8	298.5	78.6	13.3/7.1	1.01	1.028	1.04	0.479
DD3	8	1.12E-03	178.8	61.2	40.8/21.3	355.3	28.7	39.3/18.2	86.1	1.5	32/11.4	1.001	1.002	1.003	0.304
DD4	10	1.90E-02	300.1	9.6	14.5/12.2	32.1	11.2	15.8/13.4	170.4	75.1	15.1/11.7	1.015	1.007	1.023	-0.344
DD5	5	2.97E-02	169.5	13.2	25.9/11.5	262.4	12.4	25.8/14.5	34.3	71.7	18.8/7.3	1.002	1.008	1.01	0.535
DD7	10	5.66E-03	152.5	2.1	10.9/6.1	61.5	24	41.2/10.9	247.3	65.9	41.4/3.1	1.016	1.007	1.024	-0.41
DD8	6	3.30E-02	59.8	0	7/2	149.8	1.5	7.9/3.1	328.6	88.5	5.4/2.6	1.017	1.029	1.048	0.253
DD9	5	4.14E-02	248.6	17.6	8.7/5.4	158.1	1.7	8.7/2.3	62.6	72.3	5.7/2	1.005	1.03	1.038	0.687
DD10	14	4.03E-02	123.2	5.9	26.1/5.8	32.6	6.4	26.1/8.1	255.2	81.3	8.3/5.8	1.008	1.019	1.028	0.421
DD11	7	2.84E-02	258.7	5.4	26.8/5.6	350.1	14.9	26.8/8.4	149.3	74.1	8.7/5.9	1.008	1.019	1.028	0.409
DD12	17	3.92E-02	329.1	9.6	11.6/5.1	238.1	5.4	11.7/6.2	119.1	79	7.6/3.2	1.008	1.019	1.028	0.406
DD13	7	5.94E-03	217.5	1.9	14.5/2.8	127.4	3.9	15.3/7	333.8	85.7	9/2.6	1.008	1.014	1.022	0.307

N: Number of samples used for calculating mean directions. Max, Int, Min, Dec, Inc, Conf.angle: Maximum, Intermediate and Minimum axis of anisotropy tensor shown by declination and inclination with confidence angle. Ratios of mean magnetic lineation (L), magnetic foliation (F), corrected degree of anisotropy (Pj) and shape parameter (T) are also shown.

Table S3. Paleomagnetic results of the Derim Derim sills and Antrim Volcanics.

Site	N	Arcs	D [°]	I [°]	k	α_{95} [°]	Plat [°]	Plong [°]	A_{95} [°]
Derim Derim Sills									
DD1*	15/18	0	220.1	-5.0	15.9	9.2	-48.6	57.7	6.5
DD2	12/12	0	169.4	49.9	49.9	5.9	-71.1	163.2	6.5
DD-3^{+}	15/13	4	247.1	62.5	7.8	19.2	-26.4	86.1	26.5
DD-4	14/15	0	224.0	41.0	12.8	11.1	-47.6	63.1	10.5
DD-5	7/18	0	208.9	24.8	28.3	11.5	-61.9	44.5	9.0
DD-9	9/9	0	168.3	46.0	194.9	3.5	-73.1	172.4	3.6
DD-10	18/18	0	161.6	30.9	66.1	4.3	-72.2	214.6	3.6
DD-11	10/10	0	176.2	51.0	15.3	12.0	-72.5	144.8	13.3
DD-12	14/14	6	181.0	55.2	131.5	4.0	-68.7	131.8	4.8
DD-13	11/11	0	352.9	-53.8	162.9	3.4	69.2	330.7	4.0
MEAN:	8	0	183.6	46.2	17.3	13.7	-76.5	120.2	15.0
Derim Derim sills (obtained from drill cores)									
DD-7	8/8	0	107.7	40.4	82.7	5.7			
DD-8	6/6	0	348.4	54.9	392.9	3.1			

N: Number of samples used for calculating site mean directions versus obtained samples per site. Arcs: Number of incorporated great circles used to calculate mean directions (Mcfadden and Mcelhinny, 1988). Mean direction shown by declination (D), inclination (I) and precision parameter k and 95% confidence interval α_{95} (Fisher, 1953). Coordinates of palaeopole in (Plat, Plong) and the confidence interval (A_{95}). All angles are shown in degrees ([°]). $^{+}$: Site of Galiwinku dyke, not included in the MEAN calculations of the Derim Derim sills. * Site DD1 was not included in the MEAN calculations due to anomalous results compared to the remaining sites, its reddish color, and non-antipodal directions (Fig. DR4). DD-7 was obtained from the Altree-2 drill core (see main text for details) and DD-8 was obtained from drill core Tarlee-S3 (drilled by Pangaea Resources Pty Ltd.15°37’56.745’’S, 132°49’33.539’’E), but, due to missing azimuthal control, only used to verify inclination consistency.

Table S4. Lithology of Altree-2 drill core.

Age	Unit and Subunit	Height (m)	Thickness (m)
Cretaceous	Undifferentiated	Surface (0)	76
Cambrian	Tindall Limestones	73	25.5
	Nutwood Downs Volcanics	98.5	221
	Bukalara Sandstone	320	71.72
Proterozoic	Upper Velkerri Formation	391.72	280.28
	Middle Velkerri Formation	672	276.23
	Lower Velkerri Formation	948.25	281.42
	Bessie Creek Sandstones	1229.65	417.46
	Corcoran Formation	1647.11	41.12
	Derim Derim Sill	1688.23	11.62+

Table S5. Paleomagnetic poles employed in Figures 2 and 3.

#	Terr	Rockname	Abb.	Plat [°]	Plong [°]	A_{95} [°]	1234567 Q	Age Min [Ma]	Age Max [Ma]	REF
1	WAC	Gnowangerup-Fraser dykes	GF	-55.8	143.9	6.3	1111110 6	1202	1218	(Pisarevsky et al., 2014)
2	SAC	Blue Range beds & Pandurra fm	BR	-38.4	62.4	3.5	0111110 5	1300	1580	(Schmidt and Williams, 2011)
3	NAC	Mt.Isa Metamorphosed Dykes	MtI	-79	110.6	8.4	1110010 4	1500	1550	(Tanaka and Idnurm, 1994)
4	SAC	Gawler Range Volcanics	GRV	-60.4	50	6.2	0110100 3	1500	1590	(Chamalaun and Dempsey, 1978)
5	NAC	Balbirini Dolomite, upper part	Bu	-52	176.1	7.5	1110111 6	1586	1592	(Idnurm, 2000)
6	NAC	Balbirini Dolomite, lower part	Bl	-66.1	177.5	5.7	1110111 6	1606	1617	(Idnurm, 2000)
7	NAC	Emmerugga Dolomite	Em	-79.1	202.6	6.1	1111100 5	1635	1653	(Idnurm et al., 1995)
8	NAC	Tooganinie Formation	To	-61	186.7	6.1	1111111 7	1645	1651	(Idnurm et al., 1995)
9	NAC	Mallapunyah Formation	Ma	-35	214.3	3.1	1111111 7	1645	1665	(Idnurm et al., 1995)
10	NAC	West Branch Volcanics	WB	-15.9	200.5	11.3	1111100 5	1705	1712	(Idnurm, 2000)
11	NAC	Fiery Creek Formation	FC	-23.9	211.8	10.4	1110100 4	1706	1712	(Idnurm, 2000)
12	NAC	Wollogorang Formation	Wo	-17.9	218.2	7.2	1011110 5	1723	1730	(Idnurm et al., 1995)
13	NAC	Peters Creek Volcanics, upper part	PC	-26	221	4.8	1111111 7	1725	1729	(Idnurm, 2000)
14	NAC	Hart Dolerite	HD	-5.3	181	12	1111111 7	1791	1793	(Kirscher et al., 2019)
15	NCC	Liaoning and Taihang area	LT	11.3	175.8	7.6	1111111 7	1214	1225	(Ding et al., 2020)
16	NCC	Licheng LIP	LC	2.0	165.1	11.0	1111101 6	1231	1243	(Wang et al., 2020)
17	NCC	Yanliao mafic sills	Ya	-5.9	179.6	3.6	1111101 6	1316	1330	(Chen et al., 2013)
18	NCC	Tieling Fm	Ti	-11.6	7.1	6.3	1111101 6	1416	1458	(Wu, 2005)
19	NCC	Yangzhuang Fm	Ya1	17.3	214.5	5.7	0111111 6	1485	1560	(Wu et al., 2005)
20	NCC	Yangzhuang Fm	Ya2	2.4	190.4	11.9	0111111 6	1485	1560	(Pei et al., 2006)
21	NCC	Taihang dykes (Central zone)	Ta	47.9	275.2	4	1111111 7	1766	1772	(Halls et al., 2000)
22	NCC	Yinshan Dykes	Yi	32.3	248.3	2	1111111 7	1766	1772	(Halls et al., 2000)
23	NCC	Xiong'er Gp	Xi	50	272.7	4.9	1111111 7	1770	1790	(Zhang et al., 2012)
24	L	Mackenzie dykes grand mean	Mac	4	190	5	1111101 6	1265	1269	(Buchan et al., 2000)
25	L	Nain Anorthosite	NA	11.7	206.7	2.2	1110011 5	1290	1320	(Murthy, 1978)
26	L-G	Victoria Fjord dolerite dykes	VF	10.3	231.7	4.3	1111101 6	1380	1384	(Abrahamsen and Vandervoo, 1987)
27	L-G	Zig-Zag Dal Basalts	ZZ	12	242.8	3.8	1110101 5	1380	1384	(Marcussen and Abrahamsen, 1983)
28	L	St.Francois Mountains	StF	-13.2	219	6.1	1111101 6	1460	1492	(Meert and Stuckey, 2002)
29	L	Western Channel Diabase	WC	9	245	6.6	1101101 5	1587	1593	(Irving et al., 1972)
30	L-G	Melville Bugt diabase dykes	MB	5	273.8	8.7	1110111 6	1628	1638	(Halls et al., 2011)
31	L	Cleaver Dykes	CD	19.4	276.7	6.1	1111101 6	1736	1745	(Irving et al., 2004)
32	L-T-H	Deschambault Pegmatites	DP	67.5	276	7.7	1110101 5	1761	1771	(Symons et al., 2000)
33	L	Dubawnt Group	Du	7	277	8	1111110 6	1750	1820	(Park et al., 1973)
34	L-R	Martin Formation	Ma	-9	288	8.5	1101110 5	1814	1822	(Evans and Bingham, 1973)
35	L-R	Sparrow Dykes	SD	12	291	7.9	1110110 5	1823	1827	(Mcglynn et al., 1974)

Terr: Terrane: NAC (North Australia Craton), SAC (South Australia Craton), WAC (West Australia Craton), NCC (North China Craton), L (Laurentia), L-T-H (Laurentia-Trans-Hudson), L-R (Laurentia-Rae), L-G (Laurentia-Greenland). Rockname: Rock Formation/Group. Abb.: Abbreviation. Plat, Plong, A_{95}: Paleopole with according confidence interval (Fisher, 1953). 1234567 Q: Quality factors (Van der Voo, 1990). Age Min/Max: Age with uncertainty. REF: Respective reference.

Table S6. Large igneous provinces used in Figure 3.

Color	Age [Ga]	Number	LIP
Pink	Ca. 1.6	1	Gawler Range Volcanics and Olympic Dam breccia
		2	Western Channel Diabase sills and Wernecke breccia
		3	Breven-Hällefors dikes and Rapakivi intrusion
Green	Ca. 1.3	1	Derim Derim sills and Galiwinku dikes
		2	Yanliao sills
		3	Datong dikes
Orange	Ca. 1.38	1	Midsommer sills
		2	Chieress dike
		3	Victoria Land sills
		4	Hart River sills
		5	Mashak volcanics
Brown	Ca. 1.35	1	Listvyanka dike
		2	Barking Dog event, Wellington Inlier
Red	Ca. 1.26	1	Mackenzie dykes
		2	Nauyat volcanics
		3	Savage Point sills
		4	Harp dikes
		5	Lower Gardar dikes/sills
		6	Bear River dikes
		7	Central Scandinavian dolerite complex
		8	Srednecheremshanskii dike

For more information and additional references please refer to Ernst and Buchan (2001) and the webpage of the "Large Igneous Provinces Commision": http://www.largeigneousprovinces.org.

Table S7. Euler parameters for paleogeography reconstruction in Figure 3 at ~1.3 Ga.

Craton/block/terrane*	Euler Pole		Angle (°)	Reference/Source
	(°N)	(°E)		
Laurentia	12.0	135.0	+91.0	This study
WAC/SAC to NAC	-20.0	135.0	+40.0	Li and Evans (2011)
Mawson to SAC	1.3	37.7	30.3	Collins and Pisarevsky (2005)
South-East Siberia to North-West Siberia	60.0	115.0	+25.0	Evans (2009)
NAC to Laurentia	37.8	90.2	+102.7	(Kirscher et al., 2019)
NCC to Laurentia	36.9	14.6	+38.2	This study
Baltica to Laurentia	47.5	1.5	+49.0	Evans and Pisarevsky (2008)
Siberia to Laurentia	78.0	99.0	+147.0	Evans and Mitchell (2011)
Greenland to Laurentia	67.5	241.5	-13.8	Roest and Srivastava (1989)

* Rotation relative to absolute framework unless otherwise stated

REFERENCES

Abbott, S. T., Sweet, I. P., Plumb, K. A., Young, D. N., Cutovinos, A., Ferenczi, P. A., and Pietsch, B. A., 2001, Roper Region: Urapunga and Roper River Special, Northern Territory: 1:250 000 geological map series explanatory notes, SD 53-10, 11 (second ed.), Northern Territory Geological Survey and Geoscience Australia (National Geoscience Mapping Accord).

Abrahamsen, N., and Vandervoo, R., 1987, Paleomagnetism of Middle Proterozoic (C1.25ga) Dykes from Central North Greenland: Geophysical Journal of the Royal Astronomical Society, v. 91, no. 3, p. 597-611.

Buchan, K. L., Mertanen, S., Park, R. G., Pesonen, L. J., Elming, S., Abrahamsen, N., and Bylund, G., 2000, Comparing the drift of Laurentia and Baltica in the Proterozoic: the importance of key palaeomagnetic poles: Tectonophysics, v. 319, p. 167-198.

Chamalaun, F. H., and Dempsey, C. E., 1978, Palaeomagnetism of the Gawler Range Volcanics and implications for the genesis of the Middleback hematite orebodies: Journal of the Geological Society of Australia, v. 25, p. 255-265.

Chen, L. W., Huang, B. C., Yi, Z. Y., Zhao, J., and Yan, Y. G., 2013, Paleomagnetism of ca. 1.35 Ga sills in northern North China Craton and implications for paleogeographic reconstruction of the Mesoproterozoic supercontinent: Precambrian Research, v. 228, p. 36-47.

Collins, A. S., and Pisarevsky, S. A., 2005, Amalgamating eastern Gondwana: The evolution of the Circum-Indian Orogens: Earth-Science Reviews, v. 71, no. 3-4, p. 229-270.

Deenen, M. H. L., Langereis, C. G., van Hinsbergen, D. J. J., and Biggin, A. J., 2011, Geomagnetic secular variation and the statistics of palaeomagnetic directions: Geophysical Journal International, v. 186, no. 2, p. 509-520.

Ding, J., Zhang, S., Zhao, H., Xian, H., Li, H., Yang, T., Wu, H., and Wang, W., 2020, A combined geochronological and paleomagnetic study on ~1220 Ma mafic dikes in the North China Craton and the implications for the breakup of Nuna and assembly of Rodinia: American Journal of Science, v. 320, no. 2, p. 125-149.

Dunlop, D. J., 2002, Theory and application of the Day plot (M-rs/M-s versus H-cr/H-c) 1. Theoretical curves and tests using titanomagnetite data: Journal of Geophysical Research-Solid Earth, v. 107, no. B3.

Ernst, R. E., and Buchan, K. L., 2001, Large mafic magmatic events through time and links to mantle plume heads: Mantle Plumes: Their Identification through Time, no. 352, p. 483-575.

Evans, D. A. D., 2009, The palaeomagnetically viable, long-lived and all-inclusive Rodinia supercontinent reconstruction: Ancient Orogens and Modern Analogues, v. 327, p. 371-404.

Evans, D. A. D., and Mitchell, R. N., 2011, Assembly and breakup of the core of Paleoproterozoic-Mesoproterozoic supercontinent Nuna: Geology, v. 39, p. 443-446.

Evans, D. A. D., and Pisarevsky, S. A., 2008, Plate tectonics on early Earth? Weighing the paleomagnetic evidence: When Did Plate Tectonics Begin on Planet Earth, v. 440, p. 249-263.

Evans, M. E., and Bingham, D. K., 1973, Paleomagnetism of Precambrian Martin Formation, Saskatchewan: Canadian Journal of Earth Sciences, v. 10, no. 10, p. 1485-1493.

Fisher, R., 1953, Dispersion on a sphere: Proceedings of the Royal Society of London Series A: Mathematical, Physical and Engineering Sciences, v. 217, p. 295-305.

Halls, H. C., Hamilton, M. A., and Denyszyn, S. W., 2011, The Melville Bugt Dyke Swarm of Greenland: A Connection to the 1.5-1.6 Ga Fennoscandian Rapakivi Granite Province?, *in* Srivastava, R. K., ed., Dyke Swarms:Keys for Geodynamic Interpretation: Keys for Geodynamic Interpretation: Berlin, Heidelberg, Springer Berlin Heidelberg, p. 509-535.

Halls, H. C., Li, J. H., Davis, D., Hou, G., Zhang, B. X., and Qian, X. L., 2000, A precisely dated Proterozoic palaeomagnetic pole from the North China craton, and its relevance to palaeocontinental reconstruction: Geophysical Journal International, v. 143, no. 1, p. 185-203.

Idnurm, M., 2000, Towards a high resolution Late Palaeoproterozoic-earliest Mesoproterozoic apparent polar wander path for northern Australia: Australian Journal of Earth Sciences, v. 47, p. 405-429.

Idnurm, M., Giddings, J. W., and Plumb, K. A., 1995, Apparent polar wander and reversal stratigraphy of the Palaeo-Mesoproterozoic southeastern McArthur basin, Australia: Precambrian Research, v. 72, p. 1-41.

Irving, E., Baker, J., Hamilton, M., and Wynne, P. J., 2004, Early Proterozoic geomagnetic field in western Laurentia: implications for paleolatitudes, local rotations and stratigraphy: Precambrian Research, v. 129, no. 3-4, p. 251-270.

Irving, E., Park, J. K., and Donaldson, J. A., 1972, Paleomagnetism of Western Channel Diabase and Associated Rocks, Northwest Territories: Canadian Journal of Earth Sciences, v. 9, no. 8, p. 960-+.

Kirscher, U., Liu, Y., Li, Z. X., Mitchell, R. N., Pisarevsky, S. A., Denyszyn, S. W., and Nordsvan, A., 2019, Paleomagnetism of the Hart Dolerite (Kimberley, Western Australia) - A two-stage assembly of the supercontinent Nuna?: Precambrian Research, v. 329, p. 170-181.

Kirschvink, J. L., 1980, The Least-Squares Line and Plane and the Analysis of Paleomagnetic Data: Geophysical Journal of the Royal Astronomical Society, v. 62, no. 3, p. 699-718.

Kirschvink, J. L., Kopp, R. E., Raub, T. D., Baumgartner, C. T., and Holt, J. W., 2008, Rapid, precise, and high-sensitivity acquisition of paleomagnetic and rock-magnetic data: Development of a low-noise automatic sample changing system for superconducting rock magnetometers: Geochemistry Geophysics Geosystems, v. 9.

Li, Z. X., and Evans, D. A. D., 2011, Late Neoproterozoic 40 degrees intraplate rotation within Australia allows for a tighter-fitting and longer-lasting Rodinia: Geology, v. 39, no. 1, p. 39-42.

Liu, Y., Li, Z. X., Pisarevsky, S., Kirscher, U., Mitchell, R. N., and Stark, J. C., 2018, Palaeomagnetism of the 1.89 Ga Boonadgin dykes of the Yilgarn Craton: Possible connection with India: Precambrian Research.

Lowrie, W., 1990, Identification of Ferromagnetic Minerals in a Rock by Coercivity and Unblocking Temperature Properties: Geophysical Research Letters, v. 17, no. 2, p. 159-162.

Marcussen, C., and Abrahamsen, N., 1983, Paleomagnetism of the Proterozoic Zig-Zag Dal Basalt and the Midsommers0 Dolerites, Eastern North Greenland: Geophysical Journal of the Royal Astronomical Society, v. 73, no. 2, p. 367-387.

Mcfadden, P. L., and Mcelhinny, M. W., 1988, The Combined Analysis of Remagnetization Circles and Direct Observations in Paleomagnetism: Earth and Planetary Science Letters, v. 87, no. 1-2, p. 161-172.

Mcfadden and Mcelhinny, 1990, Classification of the Reversal Test in Paleomagnetism: Geophysical Journal International, v. 103, no. 3, p. 725-729.

Mcglynn, J. C., Hanson, G. N., Irving, E., and Park, J. K., 1974, Paleomagnetism and Age of Nonacho-Group Sandstones and Associated Sparrow Dikes, District of Mackenzie: Canadian Journal of Earth Sciences, v. 11, no. 1, p. 30-42.

Meert, J. G., and Stuckey, W., 2002, Revisiting the paleomagnetism of the 1.476 ga St. francois mountains igneous province, Missouri: Tectonics, v. 21, no. 2.

Murthy, G. S., 1978, Paleomagnetic results from the Nain anorthosite and their tectonic implications: Canadian Journal of Earth Sciences, v. 15, p. 516-525.

Park, J. K., Irving, E., and Donaldso.Ja, 1973, Paleomagnetism of Precambrian Dubawnt Group: Geological Society of America Bulletin, v. 84, no. 3, p. 859-870.

Pei, J. L., Yang, Z. Y., and Zhao, Y., 2006, A Mesoproterozoic paleomagnetic pole from the Yangzhuang Formation, North China and its tectonics implications: Precambrian Research, v. 151, no. 1-2, p. 1-13.

Pisarevsky, S. A., Wingate, M. T. D., Li, Z. X., Wang, X. C., Tohver, E., and Kirkland, C. L., 2014, Age and paleomagnetism of the 1210 Ma Gnowangerup-Fraser dyke swarm, Western Australia, and implications for late Mesoproterozoic paleogeography: Precambrian Research, v. 246, p. 1-15.

Roest, W. R., and Srivastava, S. P., 1989, Sea-Floor Spreading in the Labrador Sea - a New Reconstruction: Geology, v. 17, no. 11, p. 1000-1003.

Schmidt, P. W., 1993, Paleomagnetic Cleaning Strategies: Physics of the Earth and Planetary Interiors, v. 76, no. 1-2, p. 169-178.

Schmidt, P. W., and Williams, G. E., 2011, Paleomagnetism of the Pandurra Formation and Blue Range Beds, Gawler Craton, South Australia, and the Australian Mesoproterozoic apparent polar wander path: Australian Journal of Earth Sciences, v. 58, no. 4, p. 347-360.

Symons, D. T. A., Symons, T. B., and Lewchuk, M. T., 2000, Paleomagnetism of the Deschambault Pegmatites: Stillstand and hairpin at the end of the Paleoproterozoic Trans-Hudson Orogeny,

Canada: Physics and Chemistry of the Earth Part a-Solid Earth and Geodesy, v. 25, no. 5, p. 479-487.

Tanaka, H., and Idnurm, M., 1994, Paleomagnetism of Proterozoic Mafic Intrusions and Host Rocks of the Mount Isa-Inlier, Australia - Revisited: Precambrian Research, v. 69, no. 1-4, p. 241-258.

Van der Voo, R., 1990, The reliability of paleomagnetic data: Tectonophysics, v. 184, no. 1, p. 1-9.

Veikkolainen, T., and Pesonen, L. J., 2014, Palaeosecular variation, field reversals and the stability of the geodynamo in the Precambrian: Geophysical Journal International, v. 199, no. 3, p. 1515-1526.

Wang, C., Peng, P., Li, Z.-X., Pisarevsky, S., Denyszyn, S., Liu, Y., Gamal El Dien, H., and Su, X., 2020, The 1.24–1.21 Ga Licheng large igneous province in the North China Craton: Implications for paleogeographic reconstruction: Journal of Geophysical Research: Solid Earth, v. n/a, no. n/a, p. e2019JB019005.

Wu, H., 2005, New Paleomagnetic Results from Mesoproterozoic Successions in Jixian Area, North China Block, and Their Implications for Paleocontinental Reconstructions [PhD: Chinese University of Geosciences, Beijing, 133 p.

Wu, H. C., Zhang, S. H., Li, Z. X., Li, H. Y., and Dong, J., 2005, New paleomagnetic results from the Yangzhuang Formation of the Jixian System, North China, and tectonic implications: Chinese Science Bulletin, v. 50, no. 14, p. 1483-1489.

Zhang, S., Li, Z. X., Evans, D. A. D., Wua, H., Li, H., and Dong, J., 2012, Pre-Rodinia supercontinent Nuna shaping up: A global synthesis with new paleomagnetic results from North China: Earth and Planetary Science Letters, v. 353-354, p. 145-155.

Zijderveld, J. D. A., 1967, A. C. demagnetization of rocks: Analysis of results: in: Collinson, D.W., Creer, K.M., Runcorn, S.K. (Eds.), Methods in Paleomagnetism. Elsevier, Amsterdam, p. 254-286.